

## Molecular simulation of the pore size distribution effect on phase behavior of methane confined in nanopores



Bikai Jin, Ran Bi, Hadi Nasrabadi\*

Harold Vance Department of Petroleum Engineering, Texas A&M University, USA

### ARTICLE INFO

#### Article history:

Received 19 April 2017

Received in revised form

9 August 2017

Accepted 21 August 2017

Available online 25 August 2017

#### Keywords:

Pore size distribution

Phase behavior

Shale

Molecular simulation

### ABSTRACT

An understanding of the phase behavior of hydrocarbons is important in the petroleum reservoir simulation. However, fluid phase behavior in a shale reservoir is substantially different from conventional behavior. Since fluids are stored inside nanopores of shale rocks, there is a strong interaction between the pore boundary and fluid molecules. Due to this interaction, the fluid molecules are distributed heterogeneously inside the nanopores and the phase diagram is shifted under confinement. Advanced theoretical procedures such as molecular simulations are needed to properly model the heterogeneous molecular distribution inside the shale nanopores. Previous molecular simulation studies of nanoconfined hydrocarbon phase behavior have been limited to single pore size models. However, shale rocks usually have a wide pore size distribution (PSD) and single pore-size models are not accurate enough to represent a real shale system. In this work, to understand the PSD effect on the phase behavior, a recently proposed molecular simulation method, gauge-GCMC, is used to generate phase diagrams based on two types of cylindrical models (single pore and multiple pores, including one based on Eagle Ford shale rock). In single pore tests, the pore diameter is changed from 4 to 10 nm. Our results for multipore systems show that with an increasing pore size, the phase equilibrium properties approach the bulk values. Also, smaller pores cause a more significant shift in the phase diagram. Our results show that the small pores are filled before the large ones, which means that liquid will first be condensed in the small pores. In the Eagle Ford case, the pore model is designed by discretizing PSD data from experiments. The results show that it is possible to use a single pore model with a 10 nm diameter to represent the pore system of this shale sample.

© 2017 Elsevier B.V. All rights reserved.

### 1. Introduction

Knowledge of hydrocarbon phase behavior is essential in reservoir simulation, well performance evaluation, and enhance oil recovery. Several equations of state (EOS) have been proposed in the past several decades to describe the fluid properties of conventional reservoirs. However, in a shale system, the fluid phase behavior differs significantly when compared with that of conventional reservoirs. Unlike conventional rocks, shale is composed of micropores (diameter less than 2 nm), mesopores (diameter between 2 and 50 nm), and macropores (diameter larger than 50 nm) [1]. Inside the micropores and mesopores, the pore surface has an important influence on the fluid molecules. It has been proposed that liquid and vapor phases can coexist within

nanopores with the same chemical potential [2]. Based on pore-fluid interactions, the fluid molecular distribution is heterogeneous and the phase equilibrium is achieved under confinement [3].

Shale consists of pores with different diameters, which is described using a pore size distribution (PSD) [4–8]. Many techniques have been used to determine this PSD, such as small-angle and ultra-small-angle neutron scattering (SANS and USANS) [4], low pressure adsorption isotherm [4,5,8], high pressure mercury intrusion [6–8], and nuclear magnetic resonance spectrum [7]. From these studies, the PSD of shale has been found to vary between regions and samples (Fig. 1). It should be noted that the fluids can stay in an equilibrium state inside these connected pores. Thus, the PSD effect needs to be considered in a phase behavior study.

To study the confined phase behavior, a direct method is measurement through experiments. The adsorption isotherm has been widely used in previous works to calculate the confined fluid

\* Corresponding author.

E-mail address: [hadi.nasrabadi@tamu.edu](mailto:hadi.nasrabadi@tamu.edu) (H. Nasrabadi).

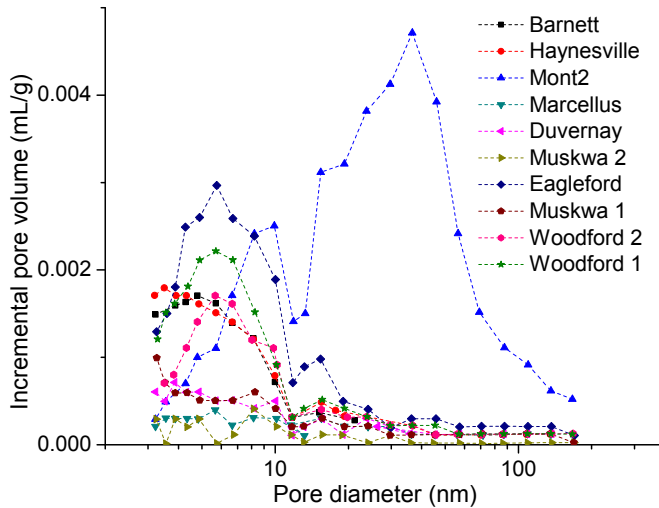


**Fig. 1.** Incremental pore volume plot for shale samples from shale gas reservoirs in North America [4].

properties [9–12]. Several nanoporous materials (e.g., controlled pore glass, MCM-41 silica) are used to generate isothermal curves. From these experiments, the critical temperature of a confined fluid is reduced while the critical density is shifted upward when compared with bulk values. Luo, Lutkenhaus, and Nasrabadi [13–16] measured the bubble points of pure and binary fluids under confinement based on the differential scanning calorimetry method. They presented an obvious shift between the bubble points in bulk and confined conditions and observed the confinement-induced supercriticality. Another device, a nanochannel chip, has been adopted in case studies of fluid flow and phase equilibrium at atmospheric pressure under confinement [17–19]. Although experimentation is a direct way to capture the confinement effect, the data is restricted by the nanoporous material, pressure and temperature conditions, and fluid samples. Most experiments are conducted using pores with a single diameter and the PSD is barely used in the experiments.

Theoretical models have also been employed in the study of nanoconfined fluids. An ideal adsorbed solution theory was presented in the simulation of an ideal gas mixture [20]. Two adsorption models, the Langmuir and Brunauer-Emmet-Teller (BET) models, have been used in studies of adsorption under confinement [21–24]. The Kelvin equation is generated to describe the pressure difference due to a curved liquid-vapor interface and is applied in studies of porous systems [25,26]. However, the hysteresis under confinement is not covered in these models [3,27].

Recently, several new applications of the EOS have been proposed in the study of confined phase behavior. Capillary pressure from the Young-Laplace equation is considered in the simulation of phase equilibrium based on the Peng-Robinson (PR) EOS [28–31]. However, the pore surface adsorption effect is not included in the assumptions, which limits the applicability of this method. In another approach, the confined critical parameters from previous molecular simulations are combined with traditional EOS applications [31–34]. This technique is restricted by those molecular simulation results. Travalloni et al. provided an extension of PR-EOS for a nanoporous system by introducing a pore size dependent term [35]. This EOS can be applied in confined phase behavior prediction when experimental data are available [15].

Monte Carlo (MC) molecular simulations have been used in confined phase behavior simulation for decades [27,36–39]. Based on the thermodynamic descriptions of interactions between

molecular particles, this method is capable of calculating the fluid properties in complex pore models. Simulations of hysteresis and the interface are also available using this statistical method. Several MC methods (GEMC [36,40,41], GCMC [42,43], gauge-GEMC [44–46], gauge-GCMC [3]) have been created for simulations in different ensembles [47,48]. Most studies have been performed using a single pore model.

In this paper, a MC molecular simulation method, gauge-GCMC from our previous work [3], is used to study the effect of PSD on the confined phase behavior of hydrocarbons. Molecular simulations are conducted for the phase diagrams of pure methane based on single pore models. Pore diameters range from 4 to 10 nm. Then, several multi-pore configurations are generated to test the PSD effect on the phase behavior, including an example based on Eagle Ford shale rock. The paper is finished with concluding remarks.

## 2. Method

### 2.1. Gauge-GCMC simulation

The gauge-GCMC method, modified from the gauge-GEMC method [44,46], is a technique for multicomponent system simulation under confinement [3]. Two boxes are involved in the simulation: one represents the fluid system and the other one is used as a gauge meter (Fig. 2). The volume of each box is fixed and several MC moves (insertion/deletion, translation and swap) are adopted during the simulation process. For a single-component fluid ( $N = 1$ ), the method is equivalent to gauge-GEMC. For a system with  $N$  components, the input parameters are: temperature  $T$ , chemical potentials ( $\mu_1, \mu_2, \dots, \mu_{i-1}, \mu_{i+1}, \dots, \mu_N$ ), and the total molecular number  $N_i$  of component  $i$ . The swap move helps the chemical potential of each component reach equilibrium between these two boxes. The insertion/deletion move keeps the chemical potentials ( $\mu_1, \mu_2, \dots, \mu_{i-1}, \mu_{i+1}, \dots, \mu_N$ ) as the input parameters.

It takes 2 million MC steps for the pure methane to reach equilibrium in single pore cases and 4 million in multiple pore systems. For Eagle Ford model 5 million MC steps are required for equilibrium. After the equilibrium, additional 1–2 million MC steps are adopted to generate the average results. Since the capacity of the gauge meter is fixed, the property of a fluid system is gradually changed and the system can stay in any state. This method can generate the complete phase diagram (e.g., density vs.  $\mu_i$ ) in the form of a van der Waals loop, including unstable, meta-stable, and stable states [44]. Phase equilibrium points are computed following the thermodynamic integration of Maxwell equal area rule [49] (Fig. 3). The critical point is extrapolated from simulation results at lower temperatures based on the rectilinear diameter law [50] and the density scaling law [51]. The density mentioned above is the average density inside pore spaces. Since fluid molecules can still move inside pores under equilibrium, it is not recommended to pick a density change in some specific regions of the model.

### 2.2. Force field

The Lennard-Jones (LJ) 12–6 potential is used to calculate the non-bonded interaction energy  $U$  between molecular particles,

$$U(r_{ij}) = 4\epsilon_{ij} \left[ \left( \frac{\sigma_{ij}}{r_{ij}} \right)^{12} - \left( \frac{\sigma_{ij}}{r_{ij}} \right)^6 \right] \quad (1)$$

where  $r_{ij}$ ,  $\epsilon_{ij}$ ,  $\sigma_{ij}$  are the separation distance, potential well depth, and finite distance where  $U$  is zero between particles  $i$  and  $j$ , respectively. The parameters ( $\epsilon/k_B$ ,  $\sigma$ ) from the TraPPE force field [52] are (148 K, 0.373 nm) for CH<sub>4</sub>, and (30 K, 0.370 nm) for

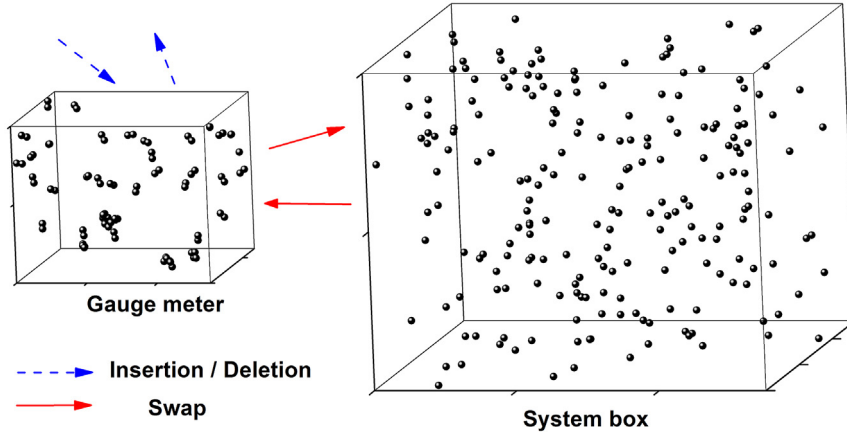


**Fig. 2.** Schematic of the gauge-GCMC method. Solid arrows represent the MC move "swap". Dashed arrows indicate the MC move "insertion/deletion".

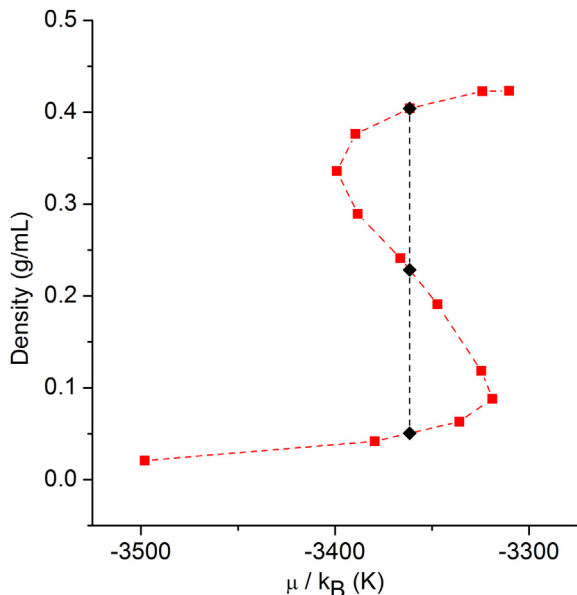


**Fig. 3.**  $\mu - \rho$  diagram of a pure ethane system in bulk. Square: results at 270 K. Diamond: equilibrium points.

aromatic carbon. The electric potential is not included for hydrocarbons since no charge is assigned. The cross potential between unlike particles are computed following the Lorentz–Berthelot combining rules [53,54]. The cutoff distance is set as 2 nm in this work based on above parameters. There is no need to include vibration, bond bending, torsion or improper torsion potentials because only methane will be discussed in this work.

### 2.3. Model

A schematic of a cylindrical model is shown in Fig. 4. A multilayer graphite model is initially generated with a layer separation of 0.335 nm in the Z direction (Fig. 4a). In each layer (X-Y plane), carbon atoms are located in a honeycomb structure with a bond length of 0.1423 nm. By cutting out redundant atoms, the single pore cylindrical model is finalized with a specific inner diameter and boundary thickness (Fig. 4b). This pore model is only applied in the system box with 1D periodic boundary condition and the gauge meter is kept in bulk situations with 3D periodic boundary condition.

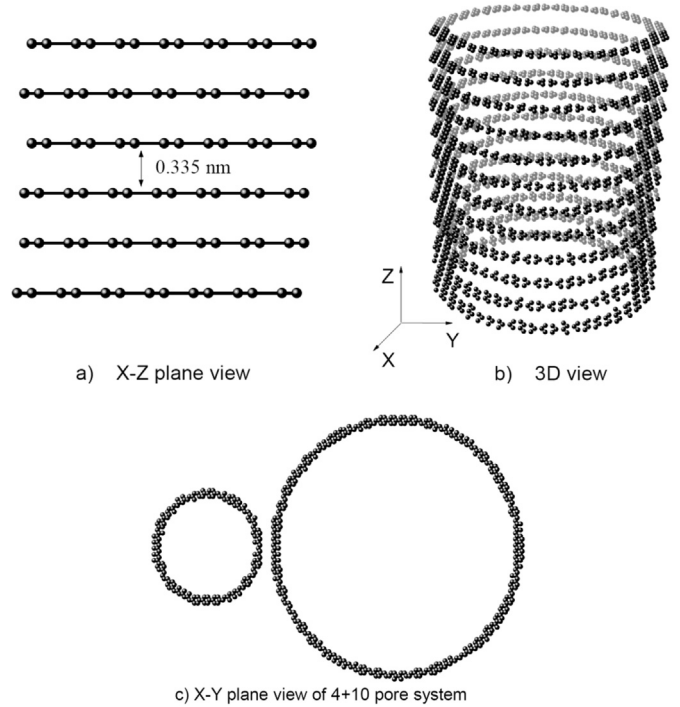


**Fig. 4.** Schematic representation of the models. a) X-Z plane view of a multilayer graphite model. The layer separation is set as 0.335 nm and the bond length is 0.1423 nm b) 3D view of a cylindrical pore with different colors for better visualization. c) X-Y plane view of a 4 + 10 parallel model. The atom size does not scale to the real values.

Based on PSD data from fields, a pore system consists of pores with different diameters. Usually, the pore length is several orders of magnitude larger than the pore diameter [6,55]. Ignoring the boundary effect at conjunction points between pores, a pore system can be treated as several single pores with specific sizes. To consider the PSD effect on the phase behavior, a multi-pore structure can be designed as parallel pores. In the parallel model (Fig. 4c), several pores are aligned in the Z direction with different diameters. This model is only included in the fluid system box and the gauge meter is still in the bulk situation. Fluids in different pores can exchange particles with each other. Since the pore separation can vary in real situations, there is no constraint regarding the spatial position relationship between pores. The parallel pore pattern was chosen because it can be simply implemented in a

simulation with 1D periodic boundary. The boundary molecules in pore  $j$  are only included in the energy calculation of fluids in pore  $j$ . There is no energy computation between the pore  $i$  and pore  $j$ . The energy is calculated separately in each pore and their summation is defined as the system energy. The system volume is defined as the total volume of single pores. In this paper, multi-pore models are named after the combination of diameters, such as "4 + 10" in Fig. 4c. To further understand the PSD effect on phase diagrams in real situations, a molecular model based on the PSD of a shale rock sample from Eagle Ford field was considered and will be explained in the next section.

### 3. Results and discussion

#### 3.1. Single pore size

The accuracy of the gauge-GCMC method has been verified in

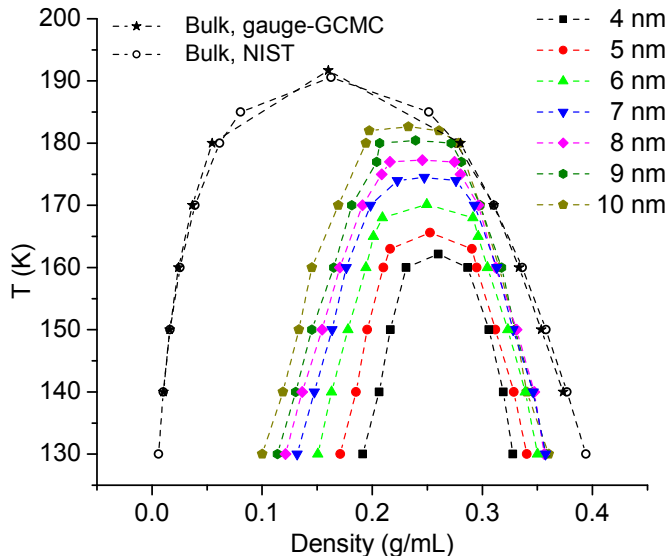


**Fig. 5.** Temperature-density diagram of methane in cylindrical models with different diameters. Empty circle: bulk data from NIST [56]. Square, circle, upward triangle, downward triangle, diamond, hexagon, pentagon: corresponding to the results of pores with diameters ranging from 4 to 10 nm, respectively. Star: simulation verification of gauge-GCMC method in bulk [3].

bulk and confined situations for pure and multicomponent fluids using slit pore models [3]. The gauge-GCMC can generate results as accurate as GCMC method. In this section, a single pore model is applied in the simulation of methane with varying diameters in the range of 4–10 nm (Fig. 5). A series of tests are conducted at the same temperature with different molecular numbers as input to generate the relationship between the chemical potential and the fluid density. By repeating the above group tests at several temperatures, phase diagrams are computed for each pore diameter as shown in Fig. 5. It is clear that the confined liquid density is reduced while the vapor density is increased in nanopores. The critical point is shifted to a lower temperature and higher density. With an increasing diameter, the phase diagram approaches its corresponding bulk values. The above confinement effects have the similar trends as observed in other work [3,27,37].

Density radius profiles of confined liquid and vapor states are generated from additional GCMC tests with calculated chemical potentials at equilibrium states. The systems are allowed to run another 2 million MC steps after the equilibrium to provide 201 snapshots which are used to calculate the radius distance of each molecule. The histograms are calculated with an interval size of 0.05 nm (Fig. 6). The distance is defined to be zero at the pore surface. In the liquid phase, there are clearly multiple adsorption layers (at least three peaks) near the pore boundary. The data for different pore sizes have a similar density distribution. As the distance from the pore wall increases, the density approaches the bulk value. Since the adsorption effect is quite weak near the center region, a fluctuation will be introduced in the local density resulting from the movement of free molecules. In the vapor state, two adsorption layers are observed, in which the first layer has values close to the corresponding peak in the liquid. Compared with profiles in small pores of both states, larger pores only extend the center region and bring little change to the distribution near the surface. It can be inferred that the densities in pores that are larger than 10 nm will have similar distributions as those shown here.

#### 3.2. Multiple pore size

To study the PSD effect on the phase behavior, multi-pore models are established as parallel pores with several diameter combinations. The parallel models are introduced in the fluid system box while the gauge meter is under bulk conditions. A series of tests are performed with increasing molecular number at several temperatures to obtain the confined phase diagrams.

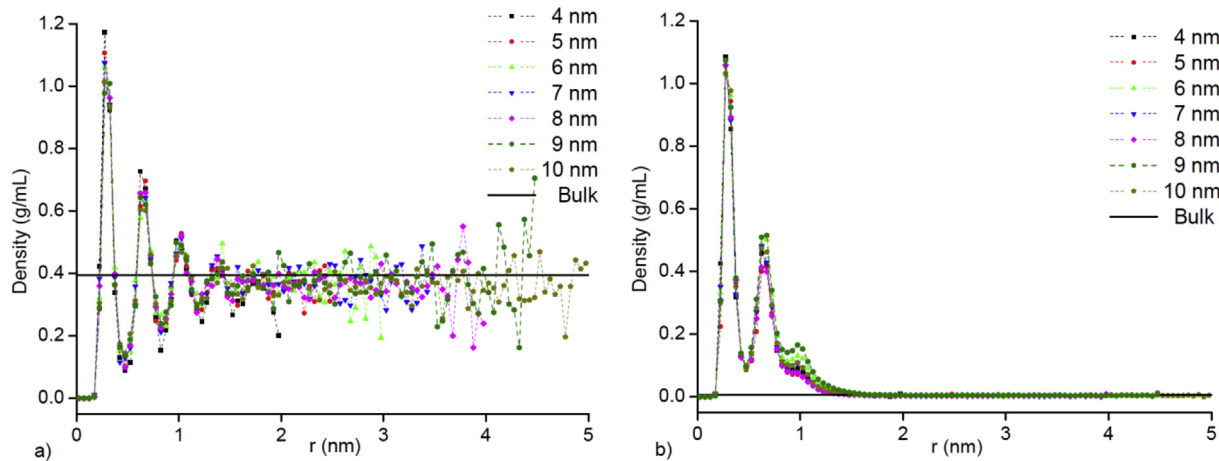


**Fig. 6.** Density radius profiles of methane at 130 K in single pores with different pore diameters. a) Liquid state, b) vapor state. Solid line: bulk data from NIST. Legends follow Fig. 5. The interval size is set as 0.05 nm in the radius direction.

### 3.2.1. 4 + 4 model

Two identical pores with a 4 nm diameter are placed parallel in the same direction with 1D periodic boundary condition. As shown in Fig. 7, the temperature-density diagram shows great agreement with the results from the single pore model. This case is conducted as a model validation to test if same-size pores have a similar influence on fluids as a single size pore (Fig. 8). From the final configurations of tests at the same temperature, these two pores are filled up at an identical pace. Two adsorption layers are observed with the trend approaching the bulk value in the center region.

### 3.2.2. 4 + 10 model

A 4 nm pore is paralleled with another 10 nm pore to form a dual-pore model. In the computation of the chemical potential and system density, the volume is defined as the summation of the internal volume of the two pores. As mentioned above, methane

molecules can communicate between these two pores and can be exchanged between the fluid system and the gauge meter. As shown in Fig. 7, the phase diagram of this model has a similar shape compared with the results for an 8 nm single pore. Even with the small deviations at lower temperatures, it can be concluded that this 4 + 10 model has similar properties as an 8 nm single pore.

Based on the correlation between the chemical potential and the fluid density (Fig. 9), the phase equilibrium points are computed using the Maxwell equal area rule [49]. To figure out the filling process in this dual-pore model, the final configurations are visualized for this case at 130 K. At the first state with a small system density in Fig. 10, the tiny pore will be filled up while the large one only has some fluid particles in the adsorption layers. By increasing the fluid density in the system, the distribution will be dense in the smaller pore and the density will reach the liquid value inside the bigger pore. This filling process agrees with the results above that phase diagrams have a larger shift in the smaller pore and liquid is first condensed in the smaller pore.

### 3.2.3. 4 + 4+10 model

To better understand the PSD effect on the phase diagram shift, a multi-pore model is designed with a combination of three diameters (4, 4 and 10 nm). As shown in Fig. 11, the phase diagram is shifted downward when compared with the 4 + 10 model with a similar form. The vapor densities increase but the liquid densities do not change significantly. It is obvious that the small pores cause a larger "shift" in the phase diagram. If one 4 nm pore is linked with a single pore system with a diameter of 10 nm, the phase diagram should be shifted downward. With more contribution from small pores (more 4 nm pores here), a greater shift in phase diagrams will be observed. If small pores of a single size take a great percentage in the PSD, confined fluid properties in the entire system will agree with results from single size pores (e.g., a 4 nm pore in this case).

From the relationship between the chemical potential and the fluid density, the phase separation is clearly shown in the van der Waals loop (Fig. 12), which is used to calculate the equilibrium properties. Based on the molecular distribution (Fig. 13) of four specific states on this  $\mu - \rho$  curve, the same trend can be concluded as in the above section that the smaller pore has the priority over the larger pore in being filled up. As the fluid density increases in

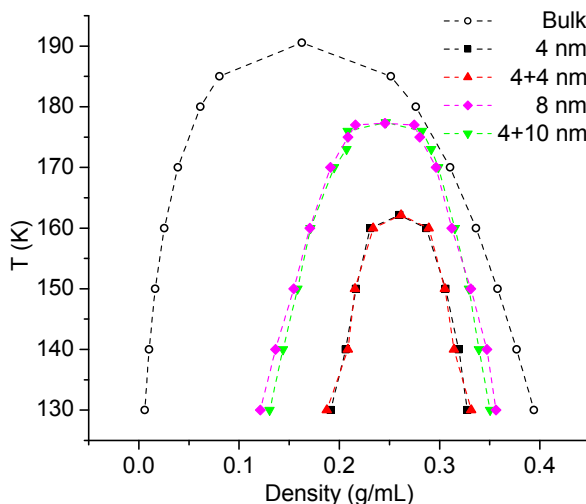


**Fig. 7.** Temperature-density diagram of methane in multi-pore models with different diameters. Empty circle: bulk data from NIST [56]. Square, diamond, upward triangle, downward triangle: corresponding to a single pore with a 4 and 8 nm diameter, and multi-pore models with diameters of "4 + 4" and "4 + 10" nm, respectively.

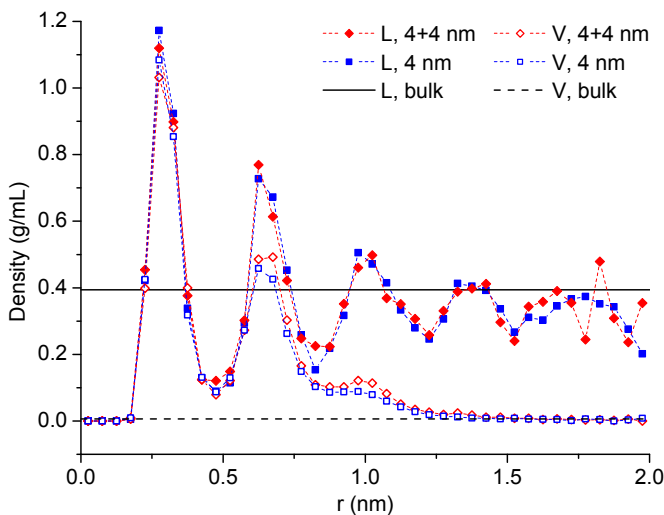


**Fig. 8.** Density radius profiles of methane at 130 K in 4 + 4 pore models. Solid line: bulk liquid data. Dashed line: bulk vapor data. Solid, empty symbols: liquid and vapor results. L: liquid state. V: vapor state. The interval size is set as 0.05 nm in the radius direction.

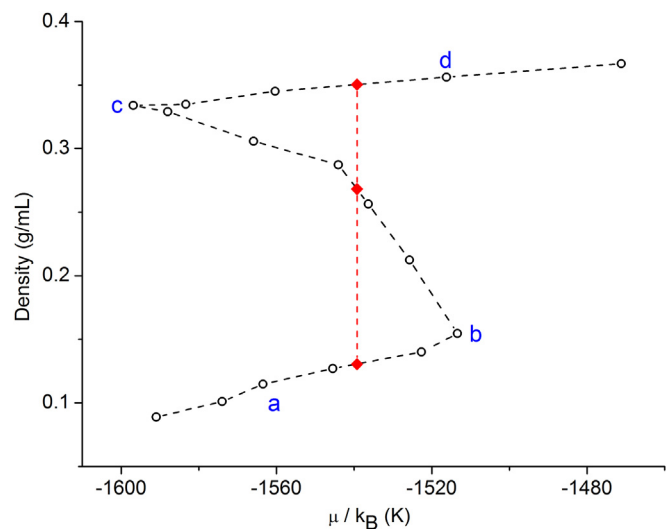


**Fig. 9.**  $\mu - \rho$  diagram for methane at 130 K in the 4 + 10 model. Molecular distributions for a) stable vapor, b) meta-stable vapor, c) meta-stable liquid and d) stable liquid are shown in the next figure. Circle: test data. Diamond: equilibrium points.

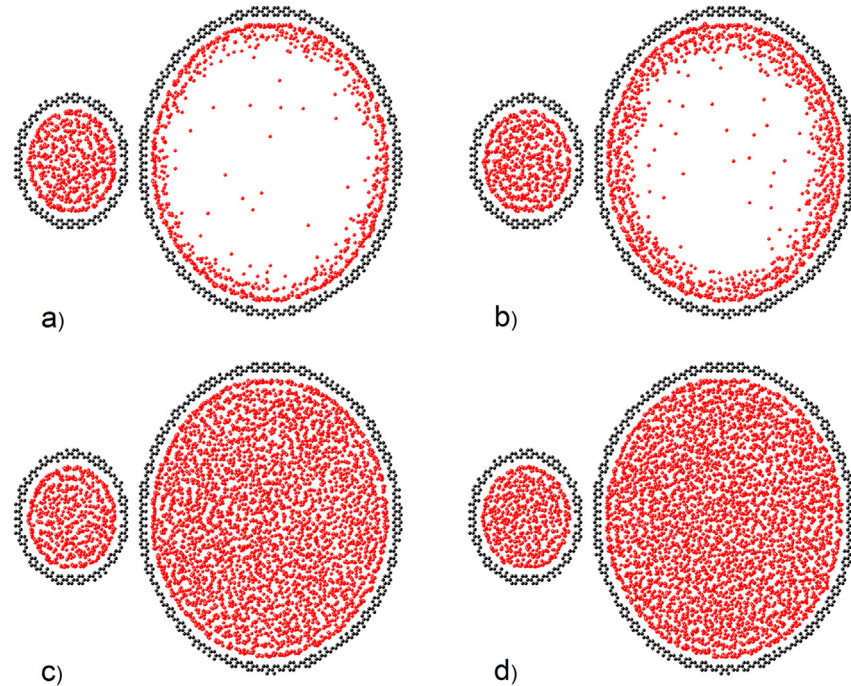


**Fig. 10.** Top views of the molecular distribution of methane at 130 K in the states a, b, c, and d from Fig. 9. Black: graphite model. Red: methane particles. (For interpretation of the references to colour in this figure legend, the reader is referred to the web version of this article.)

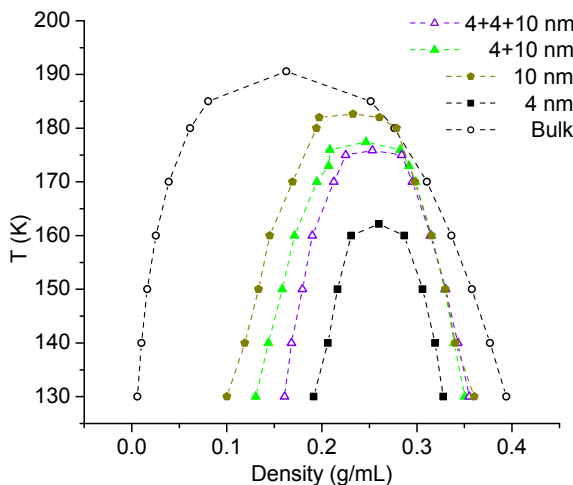


**Fig. 11.** Temperature-density diagrams for methane in multi-pore models. Empty circle: bulk data from NIST [56]. Square, solid triangle, empty triangle: 4 nm single pore, and multi-pore models with diameters of "4 + 10" and "4 + 4+10" nm, respectively.

the system, the larger pore will finally be filled and the density will increase in each pore.

### 3.3. Eagle Ford model

In this section, we will study the PSD effect on confined fluid phase behavior for an Eagle Ford shale rock sample. Eagle Ford shale is a sedimentary formation with a large amount of oil and natural gas in south Texas. It was one of the most active targets for unconventional production in U.S. in 2010. Based on the PSD data of Eagle Ford shale obtained from Hg intrusion [4], several pore sizes are chosen to represent the Eagle Ford shale sample. The selection of representative pore sizes mainly considers pores that have a

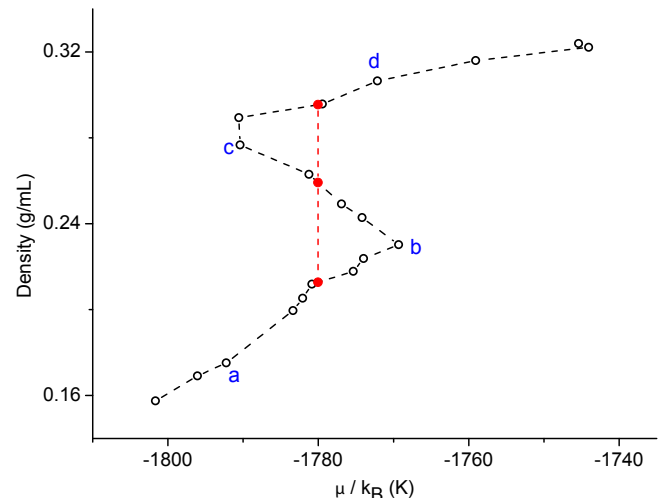


**Fig. 12.**  $\mu - \rho$  diagram for methane at 170 K in the 4 + 4+10 model. Molecular distributions for a) stable vapor, b) meta-stable vapor, c) meta-stable liquid and d) stable liquid are shown in the next figure. Circle: test data. Diamond: equilibrium points.

relatively high volume fraction and phase behavior characteristics that deviate significantly from bulk conditions. Once the representative pore sizes of the PSD are chosen, the volume fraction of each pore size can be determined by matching the area of pore sizes and volume fraction plot of the Eagle Ford sample. The measured Eagle Ford PSD from Hg intrusion [4], representative pore sizes and volume contribution of each pore are shown in Fig. 14. Pore sizes of 4, 5, 6, 8, and 13 nm are picked to represent pore sizes of 3 to 4 nm, 4 to 5 nm, 5 to 6.25 nm, 6.25 to 9 nm, and 9 to 30 nm, respectively, in the Eagle Ford sample. Due to the small volume contribution and extremely time consuming requirements of molecular simulation, we did not consider pores that have diameters more than 30 nm. Previous studies [14,19] have shown that the confinement effect

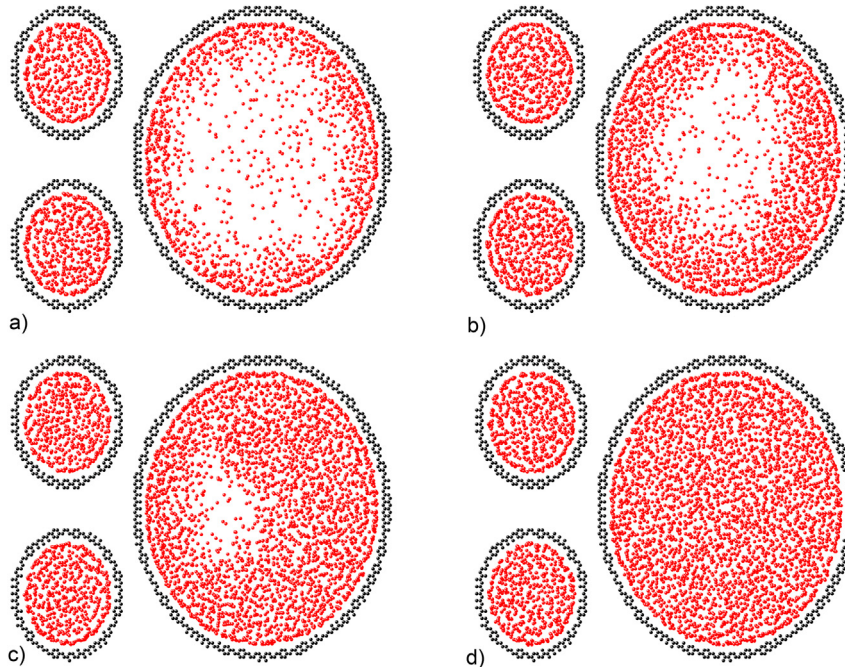


**Fig. 13.** Top views of the molecular distribution of methane at 170 K in the state a, b, c, and d from Fig. 12. Black: graphite model. Red: methane molecules. (For interpretation of the references to colour in this figure legend, the reader is referred to the web version of this article.)

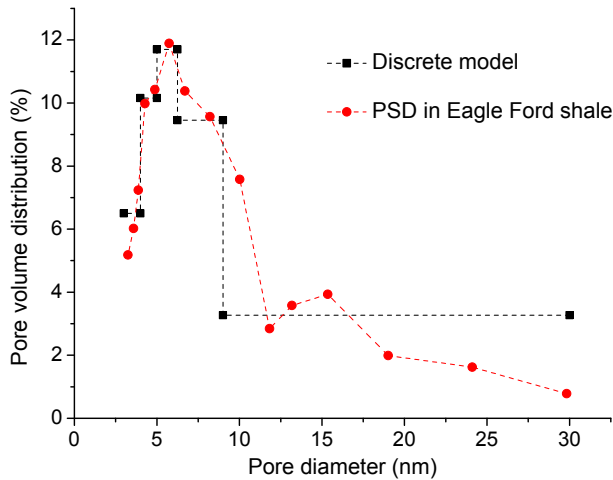


**Fig. 14.** Normalized pore size distribution of shale samples from Eagle Ford in Fig. 1 [4]. The discrete process is defined to match the area below the discrete model with the coverage below PSD curve, as mentioned in the text.

becomes negligible for such pore sizes. The final PSD model for this Eagle Ford sample was five pores independently arrayed in parallel with 1D periodic boundary condition in the Z direction. Pores are separated far enough, which means that fluid molecules in a given pore are not affected by boundary molecules in neighboring pores. The volume fraction of a pore size is defined as the summation of the pore volume with the same diameter divided by the total system volume.

Based on the results in Fig. 15, the phase diagram of this Eagle Ford sample is close to that of a 10 nm single pore model. It can be inferred that this Eagle Ford sample has an equivalent confinement effect similar to that of a single pore size of 10 nm. Simulation results of the 10 nm single pore model can be used to estimate the

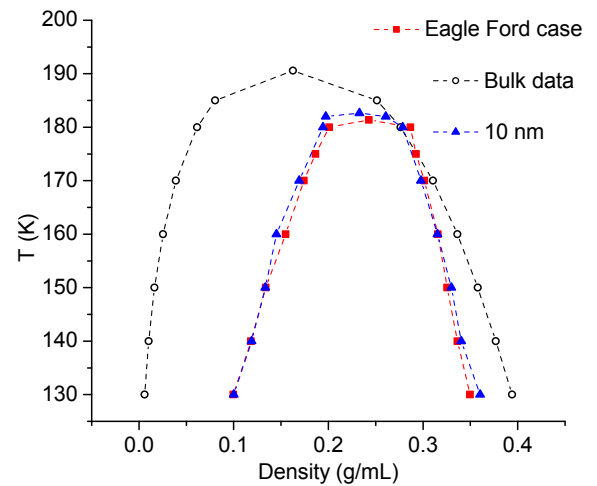


**Fig. 15.** Temperature-density diagrams for methane in an Eagle Ford pore model. Empty circle: bulk data from NIST [56]. Square, triangle: results from Eagle Ford model and a 10 nm single pore model, respectively.

phase behavior and related reservoir fluid characteristics of this Eagle Ford sample. We do not claim that it is possible to find an "effective pore radius" that can be used to model the confined phase behavior for any rock sample with a wide PSD. The existence of such a pore radius or its value requires a case-by-case analysis.

The van der Waals shape is again observed in the relationships between the chemical potential and fluid density (Fig. 16). There two diagrams are different but happens to have the close equilibrium points. The filling process follows the same rule as described above. Based on the final configurations of molecular distribution at different states (Fig. 17), the liquid will first condense in smaller pores. As mentioned in above sections, the volume of a system is the summation of the volume of each pore, and the system density

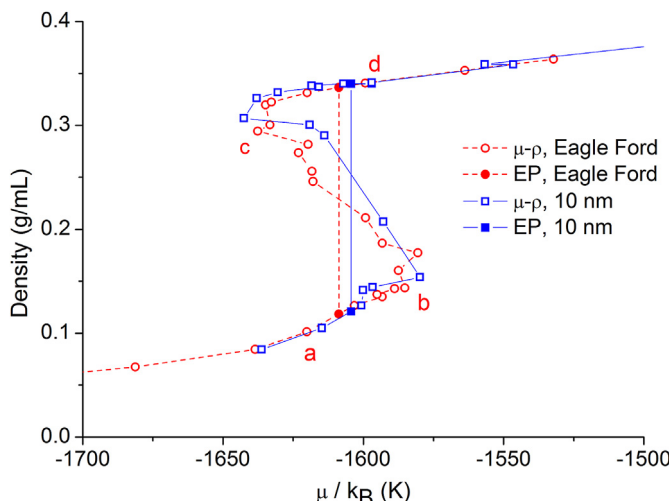


**Fig. 16.**  $\mu - \rho$  diagram for methane at 140 K in Eagle Ford and 10 nm single pore models. Molecular distribution in test a) stable vapor, b) meta-stable vapor, c) meta-stable liquid and d) stable liquid of Eagle Ford model are shown in the next figure. Circle: test data in Eagle Ford model. Square: test data in 10 nm single pore model. EP: equilibrium points.

is an average property over the whole pore spaces. During the simulation, the Eagle Ford model is treated as a black box. The phase definitions and equilibrium properties only depend on the thermodynamic relationship between the chemical potential and the system density (Fig. 16). Therefore, this condensation may happen in small pores when the system is still in vapor state (Fig. 17a). On the other hand, during the whole process, the

molecules in small pores are in dynamic equilibrium with molecules in large pores. Due to the existence of pores of other sizes, the phase behavior of the fluid in the pore of one size is not identical to that in a system with pores of only this size.

#### 4. Conclusion

In this work, the gauge-GCMC molecular simulation technique is used to investigate the PSD effect on the phase behavior of methane under confinement. The nanopores in a shale system are presented by a cylindrical model designed based on multilayer graphite. Two types of pore models (single pore and multiple pores) are considered in the molecular simulation.

In the single pore model, the confined liquid density is decreased while the vapor density is increased. The critical point has a lower temperature and a higher density under confinement. As the pore diameter is increased from 4 to 10 nm, the phase equilibrium properties approaches those of the bulk data. The smaller pore model has a stronger effect on the phase diagram shift.

In multi-pore model tests, the fluid phase diagrams are modified in the same trend as stated above. There is a great similarity between phase diagrams of the 4 + 4 model and a single 4 nm pore. For the 4 + 10 model, it is inferred that this model has similar properties as those of an 8 nm single pore. Based on the test of the 4 + 4+10 model, if the pore system has more small pores, a greater shift effect will be involved in the phase diagram. For the Eagle Ford case, a complex multi-pore model is finalized by discretizing the PSD data from experiments. This model can generate a phase diagram similar to that of a 10 nm single pore. According to all multipore model tests, it is concluded that smaller pores have priority over larger ones in being filled up, with the liquid initially being condensed in the smaller pores.

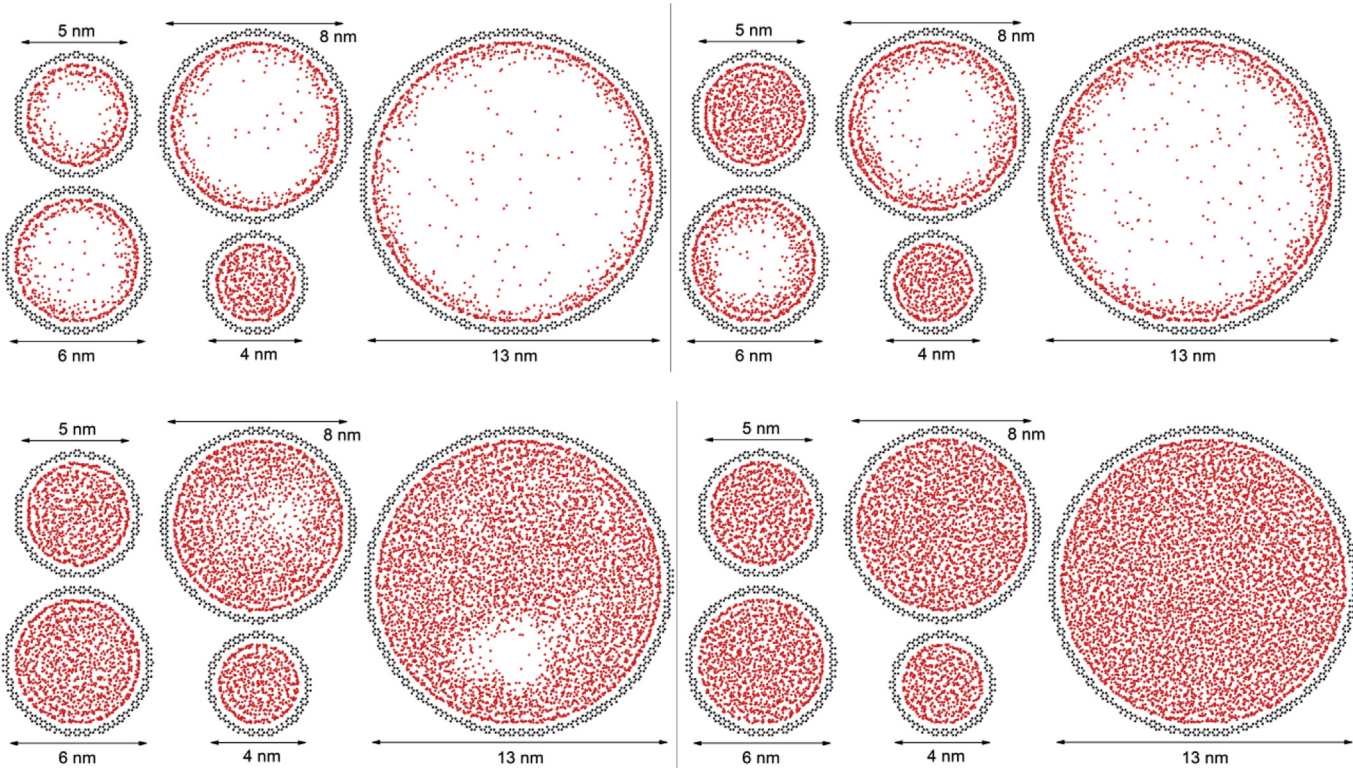


**Fig. 17.** Top views of the molecular distribution of methane at 140 K in the state a, b, c, and d from Fig. 16. Black: graphite model. Red: methane molecules. (For interpretation of the references to colour in this figure legend, the reader is referred to the web version of this article.)

## Acknowledgement

This research is supported by the Crisman Institute for Petroleum Research and High Performance Research Computing Facility in Texas A&M University. All simulations are performed based on a modified version of Monte Carlo for Complex Chemical Systems (MCCCS) Towhee [57].

## References

- [1] J. Rouquerolt, D. Avnir, C.W. Fairbridge, D.H. Everett, J.H. Haynes, N. Pernicone, J.D.F. Ramsay, K.S.W. Sing, K.K. Unger, Recommendations for the characterization of porous solids, *Pure Appl. Chem.* 66 (8) (1994) 1739–1758.
- [2] R. Evans, U.M.B. Marconi, P. Tarazona, Fluids in narrow pores: adsorption, capillary condensation, and critical points, *J. Chern. Phys.* 84 (4) (1986).
- [3] B. Jin, H. Nasrabadi, Phase behavior of multi-component hydrocarbon systems in nano-pores using gauge-gcmc molecular simulation, *Fluid Phase Equilibria* 425 (15) (2016) 324–334.
- [4] C.R. Clarkson, N. Solano, R.M. Bustin, A.M.M. Bustin, G.R.L. Chalmers, L. He, Y.B. Melnichenko, A.P. RadilAski, T.P. Blach, Pore structure characterization of north american shale gas reservoirs using usans/sans, gas adsorption, and mercury intrusion, *Fuel* 103 (2013) 606–616.
- [5] Y. Zhang, D. Shao, J. Yan, X. Jia, Y. Li, P. Yu, T. Zhang, The pore size distribution and its relationship with shale gas capacity in organic-rich mudstone of wufeng-longmaxi formations, sichuan basin, China, *J. Nat. Gas Geoscience* 1 (3) (2016) 213–220.
- [6] A.A. Hinai, R. Rezaee, L. Esteban, M. Labani, Comparisons of pore size distribution: a case from the western australian gas shale formations, *J. Unconv. Oil Gas Resour.* 8 (2014) 1–13.
- [7] R.F. Sigal, Pore-size Distributions for Organic-shale-reservoir Rocks from Nuclear-magnetic-resonance Spectra Combined with Adsorption Measurements, Society of Petroleum Engineers, 2015. SPE-174546-PA.
- [8] U. Kuila, M. Prasad, Specific surface area and pore-size distribution in clays and shales, *Geophys. Prospect.* 61 (2) (2013) 341–362.
- [9] M. Thommes, G.H. Findenegg, Pore condensation and critical-point shift of a fluid in controlled-pore glass, *Langmuir* 10 (1994) 4270–4277.
- [10] A. de Keizer, T. Michalski, G.H. Findenegg, Fluids in pores: experimental and computer simulation studies of multilayer adsorption, pore condensation and critical-point shifts, *Pure Appl. Chem.* 63 (10) (1991) 1495–1502.
- [11] L.D. Gelb, K.E. Gubbins, R. Radhakrishnan, M. Sliwinska-Bartkowiak, Phase separation in confined systems, *Rep. Prog. Phys.* 62 (1999) 1573–1659.
- [12] S.Z. Qiao, S.K. Bhatia, D. Nicholson, Study of hexane adsorption in nanoporous MCM-41 silica, *Langmuir* 20 (2) (2004) 389–395.
- [13] S. Luo, J.L. Lutkenhaus, H. Nasrabadi, Experimental study of confinement effect on hydrocarbon phase behavior in nano-scale porous media using differential scanning calorimetry, SPE-175095-MS, in: SPE Annu. Tech. Conf. Exhib., 2015.
- [14] S. Luo, J.L. Lutkenhaus, H. Nasrabadi, Use of differential scanning calorimetry to study phase behavior of hydrocarbon mixtures in nano-scale porous media, *J. Petrol. Sci. Eng.* ISSN: 0920-4105 (2016) (in press).
- [15] S. Luo, J.L. Lutkenhaus, H. Nasrabadi, Confinement-induced supercriticality and phase equilibria of hydrocarbons in nanopores, *Langmuir* 32 (44) (2016) 11506–11513.
- [16] S. Luo, H. Nasrabadi, J.L. Lutkenhaus, Effect of confinement on the bubble points of hydrocarbons in nanoporous media, *AIChE J.* 62 (5) (2016) 1772–1780.
- [17] Q. Wu, B. Bai, Y. Ma, J.T. Ok, K.B. Neeves, X. Yin, Optic imaging of two-phase-flow behavior in 1D nanoscale channels, *SPE J.* (2014) 793–802.
- [18] L. Wang, E. Parsa, Y. Gao, J.T. Ok, K. Neeves, X. Yin, E. Ozkan, Experimental study and modeling of the effect of nanoconfinement on hydrocarbon phase behavior in unconventional reservoirs, SPE-169581-MS, in: SPE Annu. Tech. Conf. Exhib., 2014.
- [19] M. Alfi, H. Nasrabadi, D. Banerjee, Experimental investigation of confinement effect on phase behavior of hexane, heptane and octane using lab-on-a-chip technology, *Fluid Phase Equilibria* 423 (2016) 25–33.
- [20] A.L. Myers, J.M. Prausnitz, Thermodynamics of mixed-gas adsorption, *AIChE J.* 11 (1) (1965) 121–127.
- [21] R.J. Ambrose, R.C. Hartman, M. Diaz Campos, I.Y. Akkutlu, C.H. Sondergeld, New pore-scale considerations for shale gas in place calculations, SPE-131772-MS, in: SPE Unconv. Gas. Conf., 2010.
- [22] R.J. Ambrose, R.C. Hartman, I.Y. Akkutlu, Multi-component sorbed-phase considerations for shale gas-in-place calculations, SPE-141416-MS, in: SPE Prod. Oper. Symp., 2011.
- [23] I. Langmuir, The constitution and fundamental properties of solids and liquids. Part I. Solids, *J. Am. Chem. Soc.* 252 (1916) 2221–2295.
- [24] S. Brunauer, P.H. Emmett, E. Teller, Adsorption of gases in multimolecular layers, *J. Am. Chem. Soc.* 60 (1) (1938) 309–319.
- [25] J.C.P. Broekhoff, J.H. de Boer, Studies on pore systems in catalysts, *J. Catal.* 9 (1) (1967) 8–14.
- [26] E.P. Barrett, L.G. Joyner, P.P. Halenda, The determination of pore volume and area distributions in porous substances. i. computations from nitrogen isotherms, *J. Am. Chem. Soc.* 73 (1) (1951) 373–380.
- [27] Z. Jin, A. Firoozabadi, Thermodynamic modeling of phase behavior in shale media, *SPE J.* (2015) 1–18.
- [28] B. Nojabaei, R.T. Johns, L. Chu, Effect of capillary pressure on phase behavior in tight rocks and shales, *SPE Reserv. Eval. Eng.* 16 (03) (2013) 281–289.
- [29] E. Parsa, X. Yin, E. Ozkan, Direct observation of the impact of nanopore confinement on petroleum gas condensation, SPE-175118-MS, in: SPE Annu. Tech. Conf. Exhib., 2015.
- [30] Y. Ma, L. Jin, A. Jamili, Modifying van der Waals equation of state to consider influence of confinement on phase behavior, SPE-166476-MS, in: SPE Annu. Tech. Conf. Exhib., 2013.
- [31] L. Jin, Y. Ma, A. Jamili, Investigating the effect of pore proximity on phase behavior and fluid properties in shale formations, SPE-166192-MS, in: SPE Annu. Tech. Conf. Exhib., 2013.
- [32] K. Sapmanee, Effects of Pore Proximity on Behavior and Production Prediction of Gas/condensate, University of Oklahoma, 2011.
- [33] D. Devegowda, K. Sapmanee, F. Civan, R. Sigal, Phase behavior of gas condensates in shales due to pore proximity effects: implications for transport reserves and well productivity, SPE-160099-MS, in: SPE Annu. Tech. Conf. Exhib., 2012.
- [34] N.S. Alharthy, T.N. Nguyen, T.W. Teklu, H. Kazemi, R.M. Graves, Multiphase compositional modeling in small-scale pores of unconventional shale reservoirs, SPE-166306-MS, in: SPE Annu. Tech. Conf. Exhib., 2013.
- [35] L. Travalloni, M. Castier, F.W. Tavares, Phase equilibrium of fluids confined in porous media from an extended pengrobinson equation of state, *Fluid Phase Equilib.* 362 (2014) 335–341.
- [36] A.Z. Panagiotopoulos, Adsorption and capillary condensation of fluids in cylindrical pores by Monte Carlo simulation in the Gibbs ensemble, *Mol. Phys.* 62 (3) (1987) 701–719.
- [37] Z. Li, Z. Jin, A. Firoozabadi, Phase behavior and adsorption of pure substances and mixtures and characterization in nanopore structures by density functional theory, *SPE J.* 19 (6) (2014) 1096–1109.
- [38] S.K. Singh, A. Sinha, G. Deo, J.K. Singh, Vapor liquid phase coexistence, critical properties, and surface tension of confined alkanes, *J. Phys. Chem. C* 113 (17) (2009) 7170–7180.
- [39] Z. Jin, A. Firoozabadi, Phase behavior and flow in shale nanopores from molecular simulations, *Fluid Phase Equilibria* 430 (2016) 156–168.
- [40] A.Z. Panagiotopoulos, Direct determination of phase coexistence properties of fluids by Monte Carlo simulation in a new ensemble, *Mol. Phys.* 100 (1) (1987) 237–246.
- [41] A.Z. Panagiotopoulos, N. Quirke, M. Stapleton, D.J. Tildesley, Phase equilibria by simulation in the Gibbs ensemble. Alternative derivation, generalization and application to mixture and membrane equilibria, *Mol. Phys.* 63 (4) (1988) 527–545.
- [42] D. Frenkel, B. Smit, Monte Carlo simulations in various ensembles, Second Ed., (chapter 5), pages 111–137, in: Daan Frenkel, Berend Smit (Eds.), *Underst. Mol. Simul.* second ed., Academic Press, San Diego, 2002.
- [43] L.A. Rowley, D. Nicholson, N.G. Parsonage, Monte Carlo grand canonical ensemble calculation in a gas-liquid transition region for 12-6 Argon, *J. Comput. Phys.* 17 (4) (1975) 401–414.
- [44] A.V. Neimark, A. Vishnyakov, Gauge cell method for simulation studies of phase transitions in confined systems, *Phys. Rev. E* 62 (4 Pt A) (2000) 4611–4622.
- [45] A. Vishnyakov, A.V. Neimark, Studies of liquid-vapor equilibria, criticality, and spinodal transitions in nanopores by the gauge cell Monte Carlo simulation method, *J. Phys. Chem. B* 105 (29) (2001) 7009–7020.
- [46] A. Vishnyakov, A.V. Neimark, Multicomponent gauge cell method, *J. Chem. Phys.* 130 (22) (2009).
- [47] A.Z. Panagiotopoulos, Monte Carlo methods for phase equilibria of fluids, *J. Phys. Cond. Matt.* 25 (2000) 25–52.
- [48] J.J. de Pablo, Q. Yan, F.A. Escobedo, Simulation of phase transitions in fluids, *Annu. Rev. Phys. Chem.* 50 (1999) 377–411.
- [49] A. Firoozabadi, *Thermodynamics of Hydrocarbon Reservoirs*, McGraw-Hill Education, 1999.
- [50] J.S. Rowlinson, F.L. Swinton, J.E. Baldwin, A.D. Buckingham, S. Danishefsky, *Liquids and Liquid Mixtures* (Third Edition). Butterworths Monographs in Chemistry, third ed., Butterworth-Heinemann, 1982.
- [51] M.P. Allen, D.J. Tildesley, *Computer Simulation of Liquids* (Oxford Science Publications), Oxford science publications. Oxford University Press, 1989 reprint edition, jun.
- [52] M.G. Martin, J.I. Siepmann, Transferable potentials for phase equilibria. 1. United-atom description of n -alkanes, *J. Phys. Chem. B* 102 (97) (1998) 2569–2577.
- [53] J.N.C. Lopes, D.J. Tildesley, Multiphase equilibria using the Gibbs ensemble Monte Carlo method, *Mol. Phys.* 92 (2) (1997) 187–196.
- [54] D. Berthelot, Sur le mélange des gaz, *Comptes rendus Hebd. des séances l'Academie des Sci.* 126 (1898) 338–340.
- [55] R. Yang, S. He, J. Yi, Q. Hu, Nano-scale pore structure and fractal dimension of organic-rich wufeng-longmaxi shale from jiaoshiba area, sichuan basin: investigations using fe-sem, gas adsorption and helium pycnometry, *Mar. Petrol. Geol.* 70 (2016) 27–45.
- [56] P.J. Linstrom, W.G. Mallard, NIST Chemistry WebBook, Natl. Inst. Stand. Technol., 2016 page NIST Standard Reference Database Number 69.
- [57] Marcus G. Martin, MCCCS Towhee: a tool for Monte Carlo molecular simulation, *Mol. Simul.* 39 (14–15) (2013) 1212–1222.